Wide versus Narrow Margins after Partial Hepatectomy for Hepatocellular Carcinoma

Preston Simmons[1], Jack Rostas[2], Dr. Robert C.G. Martin, MD, PhD[3].

[1]College of Arts and Sciences, University of Louisville; [2,3]Department of Surgical Oncology, University of Louisville

Introduction

- Despite extensive investigation, the optimal balance between oncological results and preserving parenchyma after resection of hepatocellular carcinoma (HCC) has not been clearly elucidated.
- The goal of this study was to compare the outcome after partial hepatectomy for HCC in which a margin less than or equal to 5 mm or greater than 5mm was achieved.

Methods

- A review of our prospective 2455 patient Hepato-Pancreatico-Biliary database was performed on all patients undergoing primary resection of HCC at a single center from December 2002 to April 2015.
- Patients were stratified into resection margins 5mm or less ("narrow") and those greater than 5mm ("wide").
- Primary outcome was patterns of recurrence and disease free survival (DFS)
- Unpaired t-test was used to determine if each subsequent stratification was statistically significant, with alpha set at 0.05.

Positive vs. Negative Margin

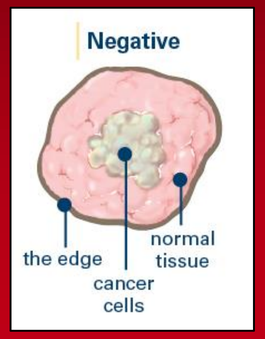

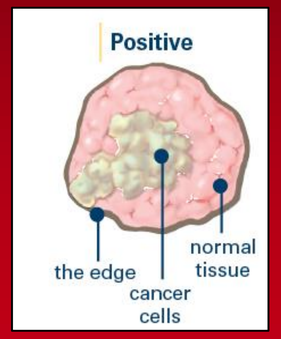

Results: Baseline and Operative

Variable	Margin Status ≤ 5 mm	Margin Status > 5 mm	p
Patients Enrolled, n	41	89	
Disease characteristics:			
Number of lesions per patient, median (range)	1 (1-20)	1 (1-10)	
Mean largest tumor size, cm (SD)	9.0 (5.6)	7.3 (4.3)	0.05
Mean resection margin, mm (SD)	2.3 (1.7)	18.0 (11.8)	0.0001*
Positive margins on final histology, n (%)	8 (19.5)	0 (0)	0.0001*
Procedure:			
Operative Time, median minutes (range)	145 (50)	125 (72)	0.09
Blood loss, mean mL (SD)	669.2 (903)	236.9 (314)	0.003*
Blood transfusion, n (%)	18 (44)	25 (27)	0.55
Length of stay, median days (range)	7 (3-22)	6 (2-32)	0.98

Results: Follow-up

Variable	Margin Status ≤ 5 mm	Margin Status > 5 mm	p
Timing of Recurrence:			
Recurrence at time of analysis, n (% total)	15 (37)	41 (46)	0.45
<1 year from resection, n (%)	9 (60)	23 (56)	1
1-2 years from resection, n (%)	3 (20)	7 (17)	1
>2 years from resection, n (%)	3(20)	11 (27)	0.73
Characteristics of recurrence			
Intrahepatic, n(%)	11 (79)	30 (75)	1
Extra-hepatic, n (%)	6 (43)	17 (43)	1
Median recurrence free survival, months	18.1	19.5	0.85
Tumor-free survival at censorship, n (%)	13 (32)	19 (21)	0.27
Median overall survival, months	34.7	37.2	0.68

Disease-free Survival

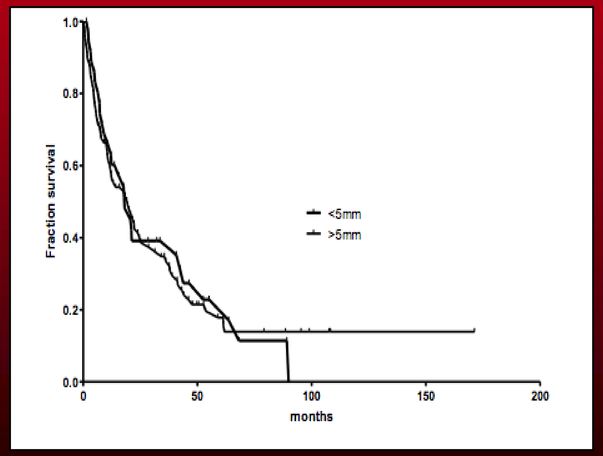

Overall Survival

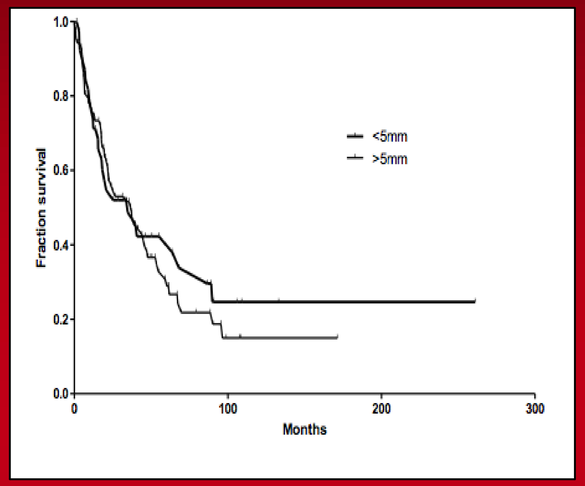

Conclusions

- A narrow resection margin (5mm or less) does not detract from the oncologic outcomes after partial hepatectomy for HCC.
- Tailoring resection margins may lead to greater preservation of hepatic parenchyma.
- Factors other than margin status represent the driving forces for local and systemic recurrence.

Acknowledgements

National Cancer Institute Grant
R25-CA134283

Effect of Hybrid Surface-Modified Nanoparticles on HPV 18 E6 Knockdown *In Vitro*

Lee B. Sims[1], Jill M. Steinbach[1]*
Department of Bioengineering[1], Principal Investigator*
University of Louisville, J. B. Speed School of Engineering

Introduction

Cancers of the female reproductive tract have a very high incidence rate, being the third leading cause of cancer-related death in women worldwide. Specifically, cervical cancer is the leading cause of death of more than 4,000 women per year in the US alone and is associated with a very high rate of late-stage diagnosis. This is attributed to the minimal symptoms associated with human papillomavirus (HPV) 16 and 18 related cervical cancer. Although there are preventative vaccines, there are few non-invasive treatments for late-stage diagnosis. To overcome this, drug delivery vehicles, such as polymer nanoparticles (NPs), can be utilized to transport non-invasive treatments by protecting agents during delivery, prolonging delivery, and safely localizing drugs and biologics to the tumor microenvironment. In addition to these attributes, NPs can be modified to significantly enhance tumor penetration and cellular internalization. In particular, the use of NP surface-modifications with both cell penetrating peptides (CPPs) and stealth ligands help to enhance NP efficacy. The long-term goals of this study were to develop poly(lactic-co-glycolic acid) (PLGA) siRNA NPs with a variety of surface modifications to: 1) therapeutically treat HPV 18 related cervical cancer and 2) evaluate how each surface modification contributes to oncogene E6 expression *in vitro*. We hypothesize that the use of a hybrid modification – combining a stealth ligand and a CPP – will increase NP efficacy by enhancing transport *through* and internalization *in* tumor cells, respectively. We expect this will cause the knockdown of E6 to induce cancer cell senescence and apoptosis.

Methods

➢ **Nanoparticle Fabrication**

In this study, we synthesized and characterized PLGA NPs encapsulating siRNA, to evaluate knockdown of HPV 18 E6. To evaluate cellular uptake, the fluorescent dye Coumarin 6 (C6) was incorporated. NPs were synthesized using an oil-in-water single or water-oil-water double emulsion technique.

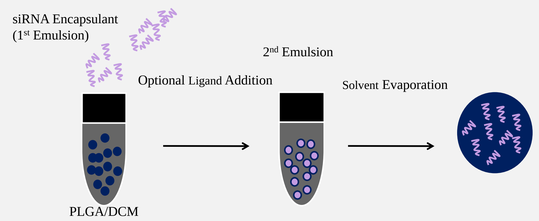

➢ **Nanoparticle Modification**

Modification of nanoparticles was achieved by incorporating avidin-palmitate into the polymer matrix and subsequently reacting with biotinylated ligands.

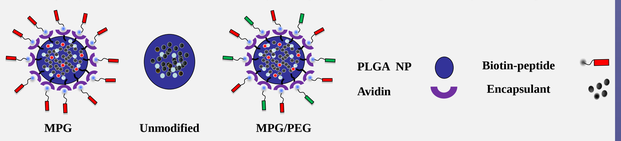

➢ **Tumor Monolayer and Spheroid Formation**

HeLa cervical cancer cells were the primary cell line used in the presented study. Tumor spheroid cultures were formed using the liquid overlay method.

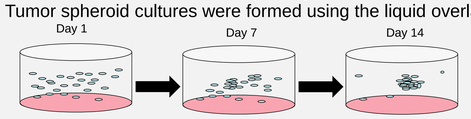

➢ **Monolayer and Spheroid NP Internalization**

Flow cytometry was used to quantify NP internalization. Spatial distribution of uptake was qualitatively verified using fluorescent microscopy. Analysis was performed at t =1.5hr and 24hr incubation.

➢ **Quantifying HPV 18 E6 mRNA Knockdown**

Cells were plated in 12-well plates, grown to 50% confluency, and were transfected with 100nM siRNA for 3 days. RNA extraction was performed using both an RNA extraction kit and Trizol reagent. RNA was subsequently purified and validated via bioanalyzer and absorption spectra from 230-280nm. Once pure, RNA was converted to cDNA and mRNA expression was determined using Real Time-PCR.

Results

Nanoparticle Characterization

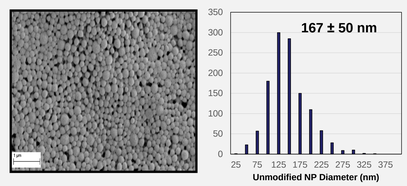

Figure 1. Scanning electron microscope (SEM) images of unmodified NPs (left) and histogram of size distribution (right).

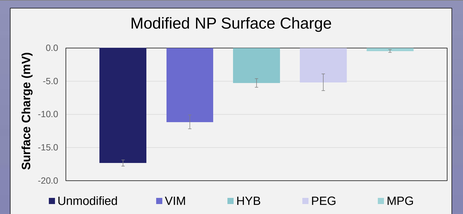

Figure 2. Nanoparticle surface charge.

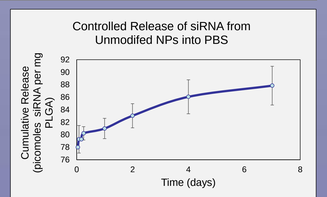

Figure 3. Cumulative release of siRNA from unmodified NPs into PBS (ongoing).

Tumor Monolayer and Spheroid Uptake and Penetration

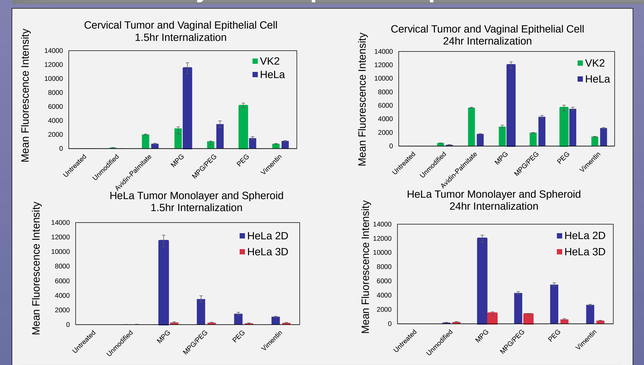

Figure 4. Flow cytometry results quantifying NP cellular internalization at 1.5hr and 24hr in monolayer HeLa and VK2 cells; and HeLa tumor spheroids.

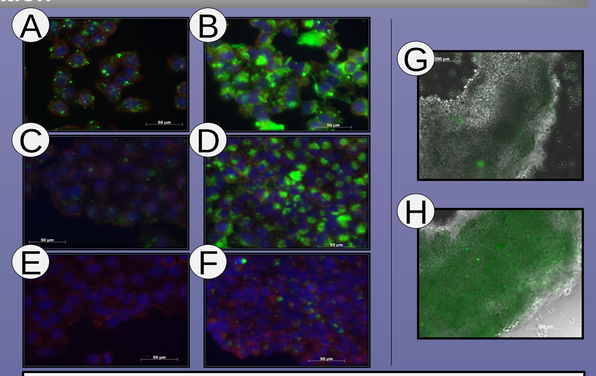

Figure 5. NP uptake in HeLa cells using confocal microscopy for: MPG (A,B); Hybrid (C,D); and unmodified (E,F); and tumor spheroid imaging using epifluorescent microscopy of unmodified (G,H) at time points 1.5hr (A,C,E,G) and 24hr (B,D,F,H).

siRNA Design

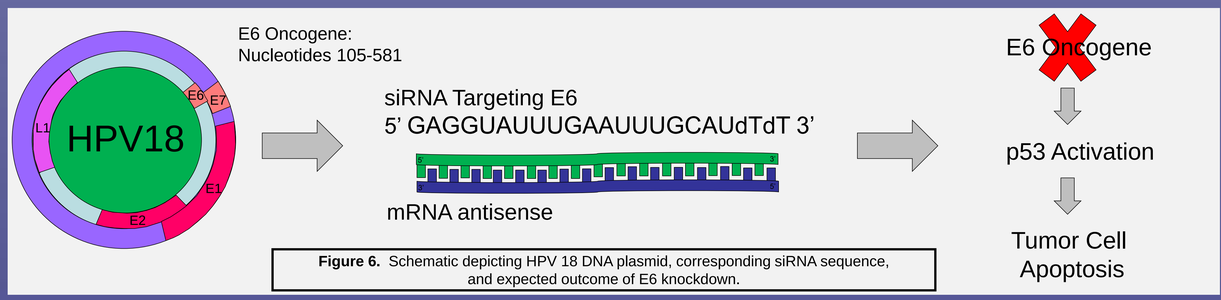

Figure 6. Schematic depicting HPV 18 DNA plasmid, corresponding siRNA sequence, and expected outcome of E6 knockdown.

HPV 18 E6 mRNA Knockdown

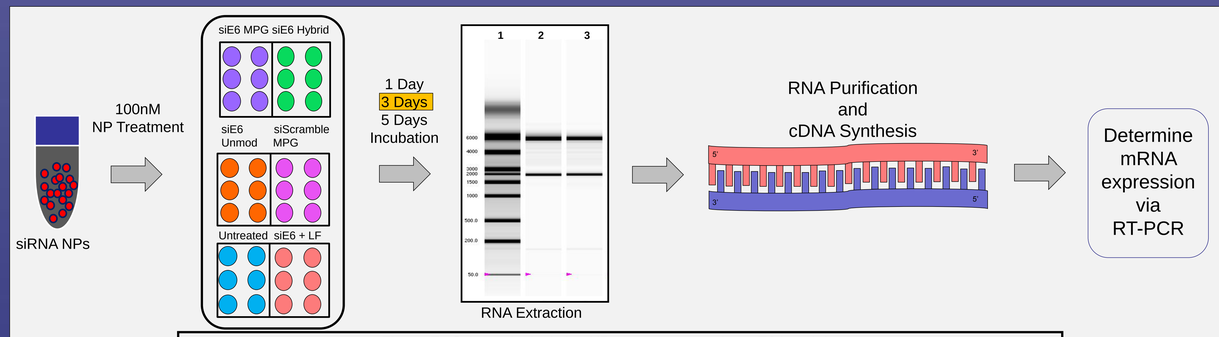

Figure 7. Schematic depicting NP treatment to evaluate E6 knockdown.
RNA extraction gel to verify RNA integrity: well 1 is the ladder and wells 2 and 3 are untreated RNA samples.

Expected (Ongoing) HPV 18 E6 Ct Values

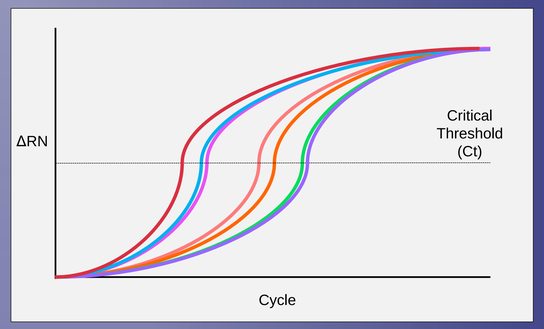

Figure 8. *Expected knockdown of HPV 18 E6 amplified on RT-PCR where GAPDH untreated, siScram+MPG, siE6+LF, siE6 unmodified, siE6+Hybrid, and siE6+MPG.

	Untreated	siScramble + MPG	siE6 + LF	siE6 + Unmodified	siE6 + Hybrid	siE6 + MPG	GAPDH
Ct Values	22	23.5	25	27	33	34	14

Table 1: *Expected critical threshold values E6 gene amplification.

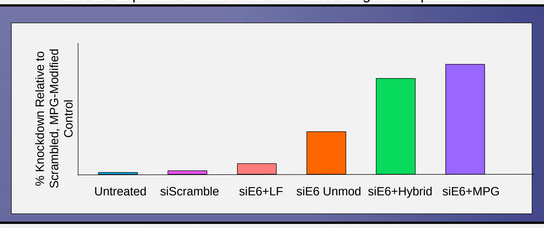

Figure 9. *Expected decrease in E6 mRNA expression based on NP treatment type.

Future Studies

- Evaluate HPV 18 E6 expression and confirm how different NP modifications affect efficacy of siRNA delivery and treatment.
- Deliver siRNA with modified NPs to treat tumor spheroids and evaluate knockdown in 3D assay.
- Test cell proliferation in both tumor monolayer and spheroid.
- Perform western blot analysis to confirm increase of tumor suppressor protein p53.

Conclusions

- MPG and hybrid-modified NPs show significantly higher efficacy in cellular internalization with both tumor monolayer and spheroid cells at both time points.
- Therefore we hypothesize that MPG and hybrid-modified NP uptake will correlate with increased delivery and siRNA knockdown efficacy of oncogene HPV 18 E6.
- PEG-modified NPs demonstrate enhanced uptake in normal VK2 cells, suggesting tumor-specific targeting. This may indicate different cell-type specific cellular uptake mechanisms.
- Twenty-four hours after NP treatment, unmodified NPs become more homogeneously dispersed throughout the tumor spheroid.
- Knockdown of HPV 18 E6 is theorized to activate tumor suppressor protein p53, resulting in an increase in cell senescence leading to tumor cell apoptosis.

Acknowledgements

Research is supported by the University of Louisville Cancer Education Program NIH/NCI R25-CA134283.

pH Specific Dual Targeting of Colloidal Mesoporous Silica Nanoparticles for Pancreatic Adenocarcinomas

Alexander Sobolev, Benjamin Fouts, Phillip Chuong, Molly McNally, Bigya Khanal, Anil Khanal, Matthew Neal, Lacey R. McNally

University of Louisville, Department of Medicine

ABSTRACT

Purpose: Even with the increased funding in research, pancreatic cancer still claims the highest mortality rate of all major cancers with the 5-year survival rate at a dismal 6%. This can be directly correlated to the inability to detect the tumors before they reach stage III and IV. The tumors are very tiny and are located deep in the body making contemporary imaging modalities unable to spot them. The combination of Multispectral Optoacoustic Tomography (MSOT) and theranostic nanoparticles offers a possible solution by providing tumor targeting using fluorescent dyes and treatment through drug delivery. In order to combat the problems faced with pancreatic adenocarcinomas, we present a colloidal mesoporous silica nanoparticle (CMSN) utilizing a chitosan coating and the V7 peptide to provide pH specific dual targeting to deliver a contrast agent.

Methods: The nanoparticle was synthesized using a modified Stober method. Water, ethanol, cetyltrimethylammonium bromide (CTAB), triethanolamine (TEA), and tetraethyl orthosilicate (TEOS) were stirred under heat for 12 hours. This formed the main structure of the nanoparticle with the CTAB and silica forming the core and the TEA acting as a complexing agent limiting aggregation. Afterwards, dialysis using a 1:1 solution of ethanol (100%) to 2M acetic acid removed the CTAB from the mesoporous silica core. Additionally, the CMSN solution was stirred with ethanol and ammonium nitrate in order to complete the scaffold removal process. Afterwards, the particles were coated with chitosan/GPTMS and then conjugated with APTES. Finally SMCC, an amine to sulfhydryl linker, joined the V7 pH low insertion peptide to the surface of the nanoparticle resulting in a dual acidic pH targeted system. Characterization was done using Transmission Electron Microscopy (TEM), UV-vis spectrophotometry (NanoDrop 200), and Zeta potential/DLS (Zetasizer Nano). To determine acidic pH specificity of V7-CMSN, Panc1 and S2VP10 cell lines were incubated in cell culture medium at either pH 7.4 or 6.6 followed by treatment with V7-CMSN. Particle uptake was determined using Near infrared fluorescence and tissue phantoms. Finally, for *in vivo* testing, the same CMSNs were injected into mice with S2VP10 pancreatic tumors. Visualization of the mice using the MSOT was performed 8 hours later.

Results: Nanoparticles were characterized using Spectrophotometry, Dynamic light Scattering (DLS), and TEM. The UV-vis readings using the NanoDrop 2000 showed very similar absorption curves for the IR-780 dye alone and the CMSN+ IR-780 dye. V7-CMSN demonstrated acidic pH specificity in both S2VP10 and Panc 1 cells at pH 6.6 that is 8X and 5X times higher than pH 7.4, respectively. In tissue phantoms, increased pH specificity was observed, 20X and 4X, respectively, using multispectral optoacoustic tomography (MSOT). Eight hours post iv injection, V7-CMSN accumulated specifically within orthotopic, tumors as observed using MSOT.

Conclusion: The acidic pH specific dual targeting system using chitosan and the pHLIP V7 resulted in tumor specificity. Preferential binding and dye release was 20X higher in pH 6.6 as compared to pH 7.4 in tissue phantoms. Also, the MSOT was able to detect tumor specific accumulation of V7-CMSN *in vivo*. The general lack of V7-CMSN binding at pH 7.4 suggests that the particle would not accumulate in off-target organs and prevent systemic accumulation.

CMSN synthesis schematic

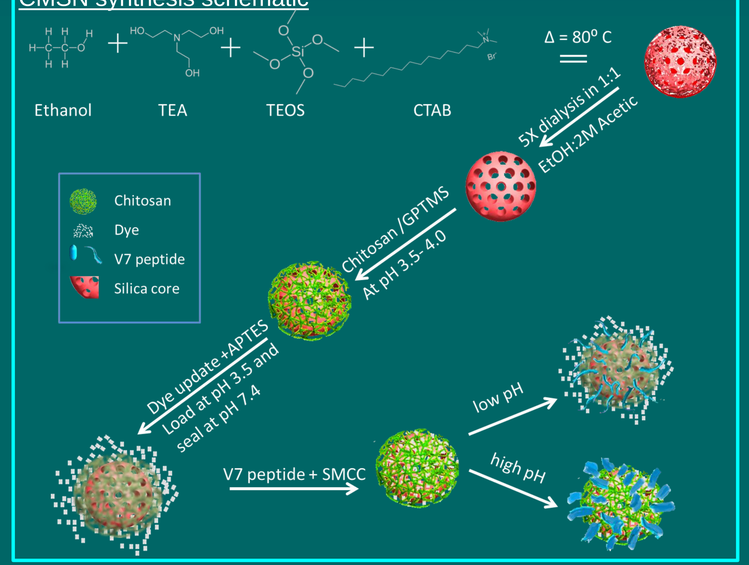

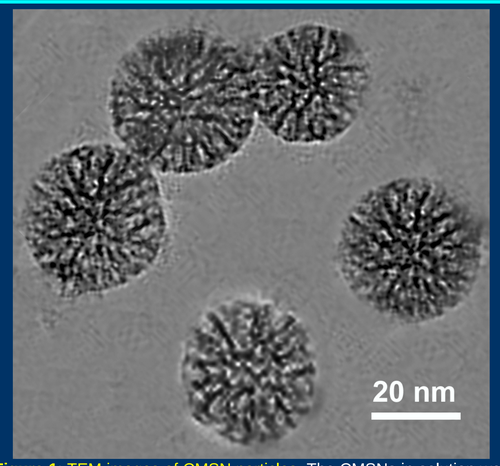

Figure 1: TEM images of CMSN particles. The CMSNs in solution were placed on a copper mesh grid and dried in order to be viewed on the Transmission Electron Microscope (TEM). The nanoparticles had a size of 32.23 ± 2.8 nm.

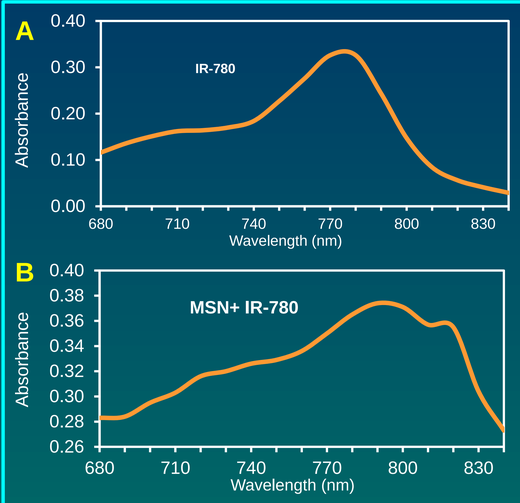

Figure 2: UV-vis spectrum of V7-CMSN + IR-780 and IR-780. The absorbance curve of the two graphs is similar, but a slight shift to the right can be noticed most likely due to the aggregation of the dye inside of the CMSN. This is known as J-aggregation. The absorbance peak for IR-780 lies around 780nm while CMSN+ IR-780 lies around 790nm.

RESULTS

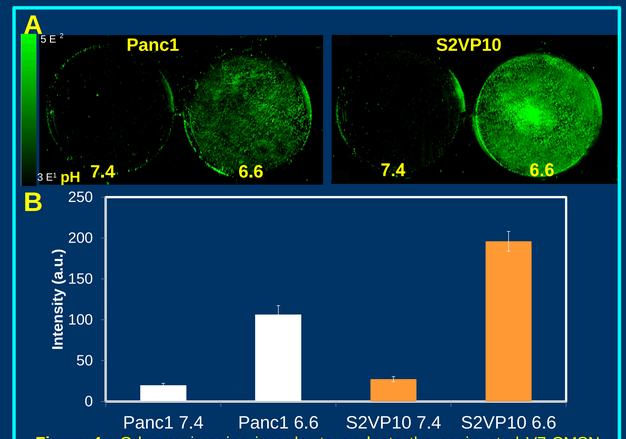

Figure 4 : Odyssey imaging in order to evaluate the conjugated V7-CMSN pH specificity *in vitro*. S2VP10 and Panc1 pancreatic cancer cells in six well plates were treated with 7.4 and 6.6 pH media and incubated with fully conjugated CMSN's for 20 min. Then the plates were washed 3X times for 10 min each using the correct pH media and imaged on the Odyssey infrared imaging system.

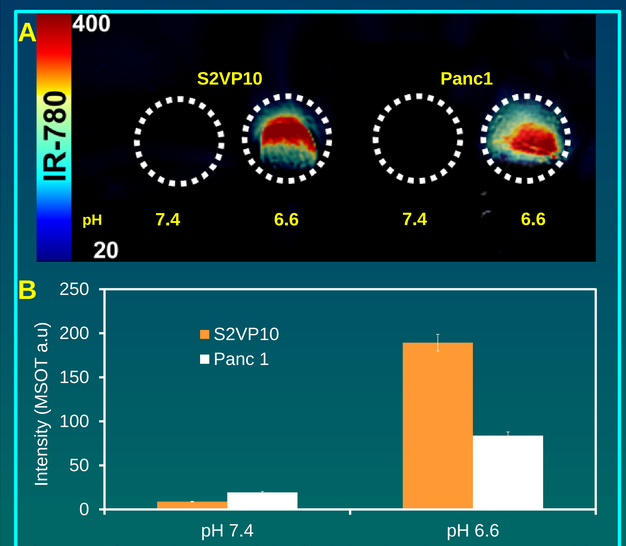

Figure 5: Tissue phantoms of dye loaded and conjugated CMSN particles. S2VP10 and Panc1 cancer cells were incubated for 20 min and washed three times. They were then scraped, centrifuged and washed again before being put into a tissue phantom (agar). The phantom was then imaged in the MSOT.

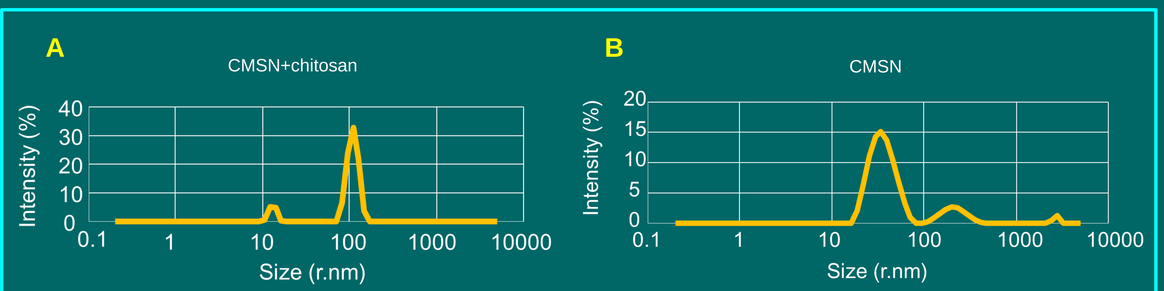

Figure 3: DLS measurements showing the addition of the chitosan coat. The intensity graphs from the Malvern Zetasizer Nano showing the distribution of size for both the CMSN with no addition and the CMSN with chitosan coating. It can be seen from the graphs that the chitosan coating increases the size of the nanoparticle drastically. However, we hypothesize that the much higher readings on the machine are due to the fact that adding a chitosan coat causes the particle to aggregate more than they usually would due to the gelatinous properties of the chitosan.

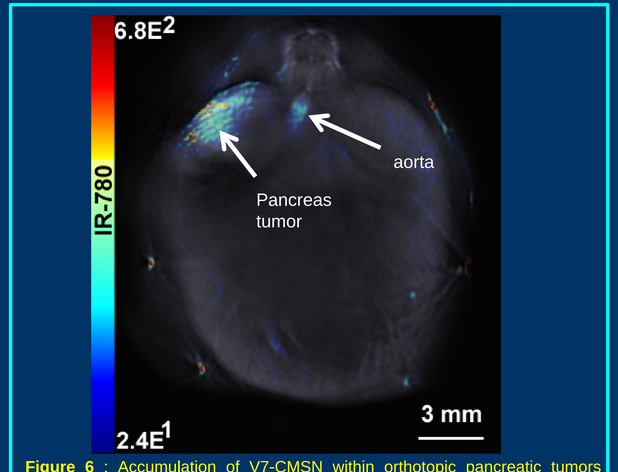

Figure 6 : Accumulation of V7-CMSN within orthotopic pancreatic tumors detected using Multispectral Optoacoustic Tomography. Athymic female mice bearing orthotopic S2VP10 tumors were injected by iv with V7-CMSNs. Mice were imaged 8h post injection and tumor specific accumulation was observed. Interestingly, liver, spleen, or kidney accumulation of V7-CMSN was not observed using MSOT.

CONCLUSION

- CMSN's coated with chitosan and conjugated with V7 demonstrate acidic pH tumor specificity in two different pancreatic cell lines, S2VP10 and Panc1.
- The MSOT imaging modality is able to detect the IR-780 dye in the bound conjugated CMSNs *in vivo*.
- The small size of the V7-CMSN improves the tumor penetration and specificity while reducing off-target accumulation.
- With improved specificity and further studies these nanoparticles could be further tested in humans in combination with the handheld MSOT to help doctors in the operating room.

FUTURE STUDIES

- Evaluating release of the IR-780 dye through dye release *in vitro* studies.
- Testing different concentrations of chitosan to achieve a smaller and more efficient coated CMSN.
- Achieving an even higher pH specificity using the V7 peptide and continuing *in vivo* imaging using the pancreatic adenocarcinoma in the mouse model
- Exploring other pH low insertion peptides for better specificity
- After further analysis, move theranostic nanoparticles using pH specificity to target tumors into clinical trials

ACKNOWLEDGEMENTS

This work was supported by NCI Grant R25-CA134283, the Brown Cancer Center High School Program, and the University of Louisville School of Medicine.

Inhibiting the Anaphase Promoting Complex/ Cyclosome: An Innovative Approach for Cancer Chemotherapy

Karen Udoh[1], J. Mason Hoffman[1], John O. Trent[2,3] J. Christopher States[1,3].

Departments of [1]Pharmacology and Toxicology and [2]Medicine, [3]Brown Cancer Center, University of Louisville, Louisville, KY

Abstract

The anaphase promoting complex/cyclosome (APC/C) is a large, E3 ubiquitin ligase that regulates the cell cycle, in particular the metaphase to anaphase transition in mitosis and the re-entry into G1 phase. Inhibition of the APC/C results in mitotic arrest and apoptosis in cancer cells. ANAPC2 and ANAPC11 are shown to be two vital subunits for APC/C function. in silico screening of ANAPC2 identified compounds that are predicted to prevent the association of ANAPC2 and ANAPC11. Thus, we hypothesize that the relative levels of the APC/C molecular targets, securin and cyclin B, will increase in cells treated with lead compounds. To gain better insight on the inhibition of the APC/C in cancer cells, HeLa cells were treated with lead compounds 3, 8, 10, and 11 at their respective IC50s for 24 h and then harvested to make lysates. The Bradford Protein Assay was used to determine the protein concentrations in each of the samples. To examine the relative levels of securin and cyclin B, a western blot analysis was performed. Results showed that cells treated with compounds 3, 8, 10, 11 do not have increased levels of securin and cyclin B. However, future analysis may reveal that treatment with the lead compounds causes a decrease in the levels of ubiquitinylated cyclin B and securin. This research was supported in part by University of Louisville Cancer Education Program NIH/NCI grant R25-CA134283 and a Kentucky Lung Cancer Research Program grant to JCS.

Introduction

- Adjuvant chemotherapy has increased cancer survival rate
- However, people are still dying from this disease, justifying the need for new chemotherapeutics
- Taxanes are chemotherapeutics that disrupt microtubule function, leading to mitotic arrest and apoptosis in cancer cells
- However, taxanes like pacitaxel and docetaxel are known to be ineffective with cancer cells lacking functional Spindle Assembly Checkpoints or containing mutant tubulin and are often in short supply
- This project is directed towards developing new mitosis disrupting drugs

The Anaphase Promoting Complex/ Cyclosome (APC/C)

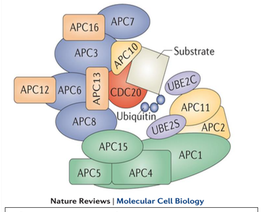

Figure 1. APC/C Structure
The APC/C is an E3 ubiquitin ligase that regulates the cell cycle. It contains 14 different subunit proteins and two co-activator subunits: Cdh1 and Cdc20. APC/C function is vital for cell proliferation and inhibition of the APC/C results in mitotic arrest and apoptosis in cancer cells.

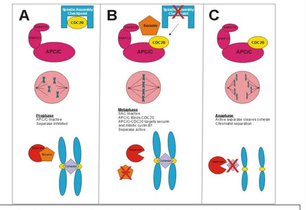

Figure 2. Model of the APC/C and Spindle Assembly Checkpoint (SAC) during Mitosis
Prophase: The SAC inhibits Cdc20 binding of the APC/C, preventing degradation of two important molecular targets, cyclin B and securin. Securin inhibits separase. Cohesins hold the sister chromatids together.
Metaphase: The Cdc20 is released and binds to the APC/C. Activated APC/C-Cdc20 complex ubiquintinylates cyclin B and securin for degradation. This allows for separase to be activated. **Anaphase:** Separase cleaves the cohesins of the sister chromatids for separation. (Figure provided by Douglas J. Saforo)

- Homology structure of ANAPC2 was screened *in silico* against a small compound library to identify lead compounds to inhibit complex formation.
- The ability of lead compounds to stabilize APC/C targets was determined.

Hypothesis

If lead compounds bind to ANAPC2 and inhibit the binding of ANAPC11, thus the APC/C molecular targets, cyclin B and securin, will accumulate in the treated cells.

Materials and Methods

Step 1

Lead Compounds:

These 4 compounds were dissolved in DMSO solution.

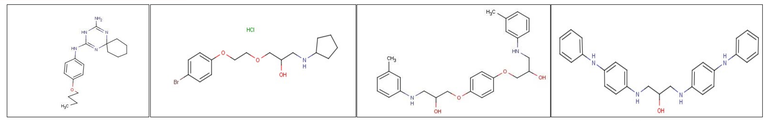

3 8 10 11

Cell Culture:

HeLa cells were plated in 6 cm dishes and were allowed to attach at the same time.

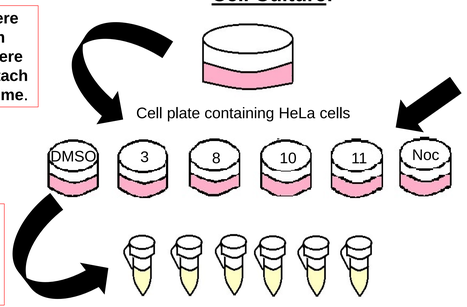

Cells were treated with compounds 3, 8, 10 & 11 at their IC50s and Nocodazole (90 ng/µL) for 24 h.

Cells were harvested and protein extracts were prepared.

Step 2

Bradford Protein Assay:

Conducted to determine protein concentration of lysates.

Step 3

Western Blot Analysis:

Performed Western Blot to detect levels of securin and cyclin B extracted from HeLa cells

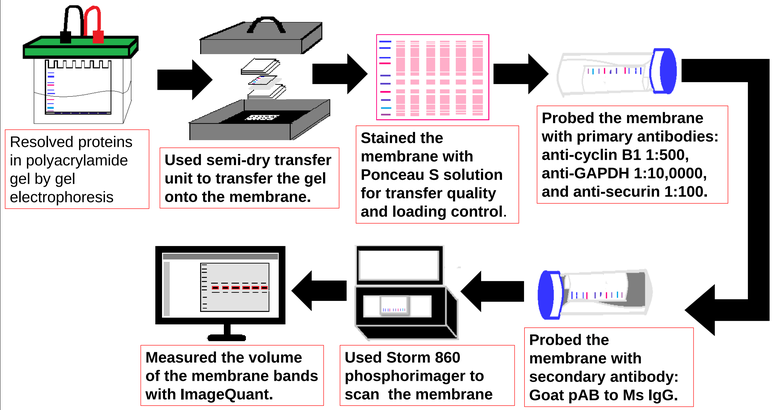

Resolved proteins in polyacrylamide gel by gel electrophoresis

Used semi-dry transfer unit to transfer the gel onto the membrane.

Stained the membrane with Ponceau S solution for transfer quality and loading control.

Probed the membrane with primary antibodies: anti-cyclin B1 1:500, anti-GAPDH 1:10,0000, and anti-securin 1:100.

Probed the membrane with secondary antibody: Goat pAB to Ms IgG.

Used Storm 860 phosphorimager to scan the membrane

Measured the volume of the membrane bands with ImageQuant.

Results

Fig. 3

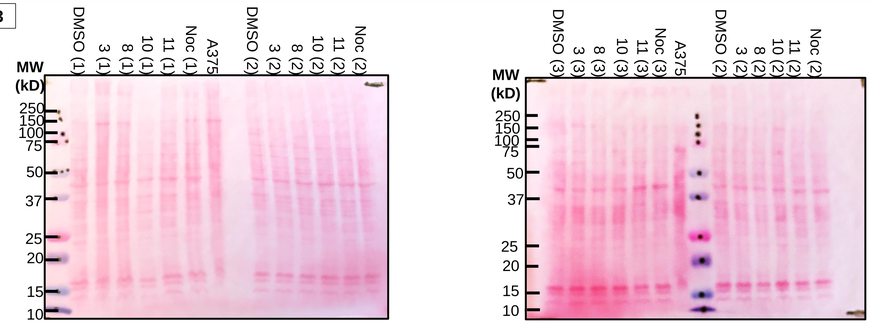

Figure 3. Ponceau-S Stained blots
Membranes were stained in Ponceau S solution for 10 minutes on a shaker after proteins were transferred. They correspond to blots in Figure 4.

Fig. 4

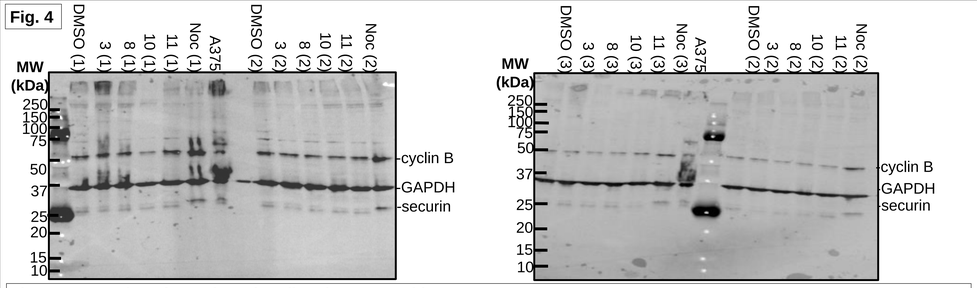

Figure 4. Detection of securin and cyclin B by Western blot.
Proteins extracted from three biological replicates of HeLa cells treated with compounds 3, 8, 10, 11, or Nocodazole were resolved by SDS-PAGE (12%), then transferred onto nitrocellulose membranes and probed with purified mouse anti-cyclin B and anti-GAPDH antibodies for 1 h each at room temperature. Then the membrane was probed with purified mouse anti-securin for 24 h at 4°C., followed by Goat pAB to mouse IgG secondary antibody conjugated to horseradish peroxidase for 1 h at room temperature. Bands were visualized by incubating in ECL plus and scanned on Storm 860 phosphorimager in fluorescence mode. Bands detected: securin at 26 kDa, GAPDH at 36 kDa, and cyclin B at 48 kDa.

Fig. 5

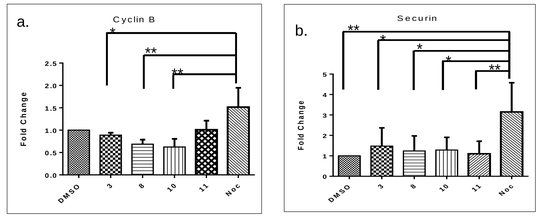

Figure 5. Western Blot Quantification.
The graphs show the fold change of **a)** cyclin B and **b)** securin in the three biological replicates. Cyclin B and securin were normalized to GAPDH. Significance was tested by one-way ANOVA ($p<0.05$). Means ± S.D were plotted. Asterisks (*, **) indicate significance with Tukey's Multiple Comparison Test. **a)** Noc compared with 3, 8, and 10 showed significance. **b)** Noc compared with DMSO,3, 8, 10 and 11 showed significance.

Conclusions

- There was no substantial change between the relative levels of cyclin B and securin in the HeLa cells treated with the lead compounds.
- Cyclin B and securin were stabilized by nocodazole.
- These data suggest that lead compounds 3, 8, 10, and 11 are not inhibiting the APC/C, under these conditions.

Acknowledgements

This research was supported in part by University of Louisville Cancer Education Program NIH/NCI grant R25-CA134283 and Kentucky Lung Cancer Research Program grant to JCS.

TARGETING ATP-BINDING CASSETTE TRANSPORTER (ABCB5) IN BRAF INHIBITOR RESISTANT MELANOMA

JINGJING XIAO, HONGYING HAO, M.D., PH.D., KELLY M. MCMASTERS, M. D., PH. D.
DEPARTMENT OF SURGERY, UNIVERSITY OF LOUISVILLE SCHOOL OF MEDICINE

Abstract

Melanoma is the most dangerous form of skin cancer. More than 50% of metastatic melanoma patients have a specific mutation in the serine/threonine kinase BRAF. This results in constitutive activation of the RAS-RAF-MEK-ERK-MAP kinase pathway, which causes uncontrolled cell growth. Vemurafenib (also known as PLX4032) is an oral chemotherapy agent that targets the specific mutation V600E in the BRAF protein. It has shown very promising results, but melanoma cells rapidly develop resistance to the BRAF inhibitor PLX and disease progression ensues. The mechanisms by which melanomas develop BRAF inhibition resistance remain unknown, but the overexpressed ABCB5 oncoprotein, an ATP-binding cassette (ABC) transporter, has been shown to efflux anti-cancer drugs from melanoma. We hypothesize that ABCB5 contributes to the PLX resistance of melanomas by effluxing anti-cancer drugs. Our goal is to determine whether ABCB5 is highly expressed in BRAF inhibitor resistant melanoma cells and to demonstrate that inhibition of ABCB5 may overcome BRAF inhibition resistance. We first established three PLX resistant melanoma cell lines, SK-28PLX, A2058PLX, and A375PLX. We showed that ABCB5 was overexpressed in SK-28PLX and A2058PLX cells, but not A375PLX cells, and that ABCB5 overexpression is associated with activation of p-ERK status. Knockdown of ABCB5 by siRNA resulted in the re-sensitizing of PLX in A2058PLX resistant cells. These results confirm that overexpression of ABCB5 may be one of the causes for resistance to the BRAF inhibitor in melanoma cells. It provides a starting point for personalized treatment strategy in targeting ABCB5 in BRAF inhibitor resistance melanomas.

Introduction

❖ Why ABCB5?

ATP-binding cassette (ABC) transporters are associated with multidrug resistance

- Efflux anticancer drugs from cells
- Serve as a melanoma stem cell marker
- Drive melanoma initiation and progression

❖PLX4032 inhibits BRAF

❖So, is ABCB5 related to PLX resistance?

❖Can we target ABCB5 to control PLX resistance?

Analyzing ABCB5 mechanism in melanoma chemoresistance could lead to new therapeutic strategies.

Methods

1. PLX resistant melanoma cell lines were established. IC50 values of PLX resistant melanoma cell lines were determined by MTT.
2. ABCB5 and ERK expression were checked with RT-PCR and Western Blots in PLX sensitive and PLX resistant cell lines.
3. ABCB5 was knocked down using siRNA transfection. ABCB5 levels were confirmed using real time RT-PCR.
4. Chemoresistance reversal assays were conducted to check for re-sensitization to PLX in PLX resistance cell lines.

Results

BRAF mutation cell lines	Culture in PLX 4032	BRAF inhibitor resistant cell lines
SK-MEL-28	0.5μM	SK-MEL-28 PLX
A2058	10μM	A2058 PLX
A375	1μM	A375 PLX

Figure 1. Establishment of PLX resistant melanoma cell lines.

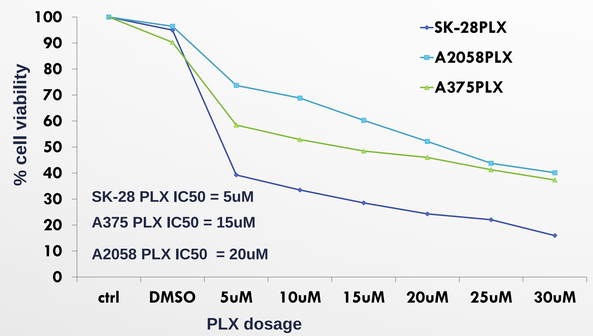

Figure 2. IC50 determination in PLX resistance melanoma cells.

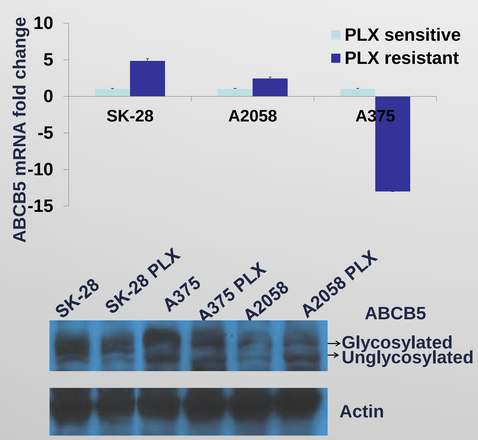

Figure 3. Differential expression of ABCB5 in 3 PLX resistant cell lines by real time RT-PCR and Western Blot.

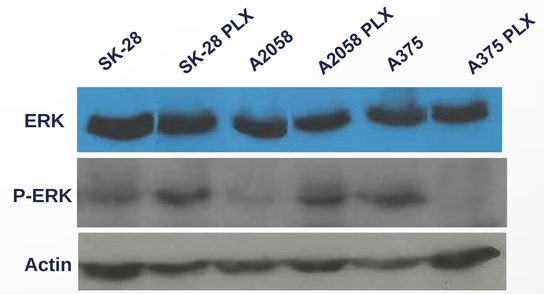

Figure 4. Differential expression of ERK and p-ERK in three PLX resistant cell lines.

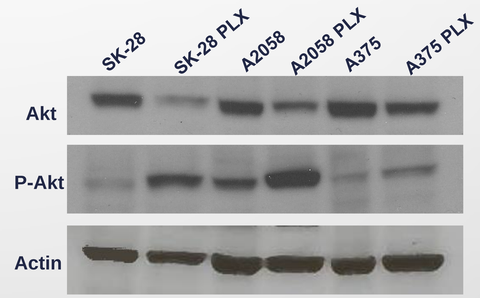

Figure 5. Downregulation of Akt and upregulation of p-Akt in three PLX resistant cell lines.

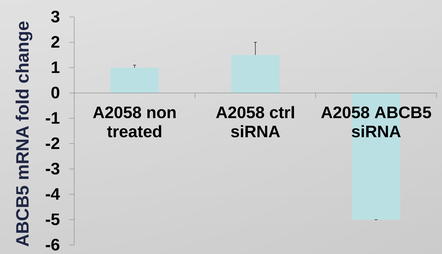

Figure 6. ABCB5 knockdown in A2058PLX cell line by real time RT-PCR.

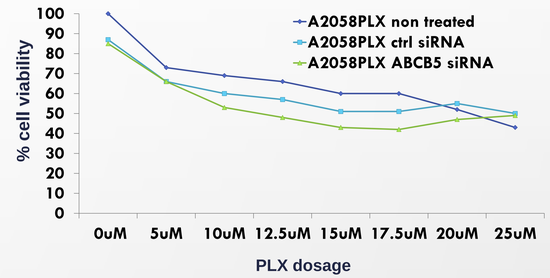

Figure 7. PLX re-sensitization after ABCB5 knockdown in A2058 PLX resistant cell line.

Conclusions

- ABCB5 was differentially expressed in PLX-resistant melanoma cell lines.
- ABCB5 upregulation in PLX-resistant cell lines may not be associated with Akt and p-Akt level.
- ABCB5 upregulation in PLX-resistant cell lines may be associated with p-ERK levels.
- ABCB5 knockdown in PLX resistant cells may re-sensitize PLX resistant cells to PLX.
- These findings may lead to personalized treatments for chemoresistant melanoma.

Future directions

- Examine effect of ABCB5 knockdown in SK-28 PLX cell lines
- Examine change in ERK and p-ERK levels after ABCB5 knockdown
- Evaluate association between ABCB5 expression and drug resistance
- Differentiate the roles of glycosylated and unglycosylated ABCB5 in chemoresistance

Acknowledgements

This research was supported by NCI R25 grant to the University of Louisville Cancer Education Program NIH/NCI (R25-CA134283).

I am grateful to the Cancer Education Program and the McMasters's Lab of the University of Louisville for their support.

UNIVERSITY OF LOUISVILLE
It's Happening Here.

Exploring Energy Metabolism Changes in Vinyl Chloride Induced Non-Alcoholic Fatty Liver Disease (NAFLD)

Heegook Yeo[1], Lisanne C. Anders[1], Adrienne M. Bushau[1], Brenna Kaelin[1], Gavin E. Arteel[1], Matthew C. Cave[1,2,3], Craig J. McClain[1,2,3] and Juliane I. Beier[1]

[1] Department of Pharmacology and Toxicology, [2] Department of Medicine, University of Louisville Health Sciences Center, Louisville KY 40292, USA, [3] Louisville VAMC

ABSTRACT

Background. Vinyl chloride (VC) is a ubiquitous environmental contaminant and ranks 4th on the ATSDR Hazardous Substances Priority List. We have previously reported increased hepatocellular necrosis in a highly exposed occupational cohort and in vitro models. A major paradigm shift in environmental research is to assess the impact of underlying disorders that may modify risk. Arguably, the most ubiquitous underlying disorder in the developed world is obesity. The impact of obesity and obesity-induced liver damage (i.e., NAFLD) on hepatic injury caused by VC is not known. The purpose of the current study was to investigate hepatic injury caused by chloroethanol (ClEtOH; VC metabolite) and the changes in carbohydrate and lipid metabolism in an experimental model of high-fat diet (HFD) induced obesity.

Methods. Mice were administered a bolus dose of chloroethanol (or vehicle) 10 wks after being fed an HFD (42% milk fat)-fed or low fat control diet (LFD; 13% milk fat). Animals were sacrificed 0-24 hours after ClEtOH exposure. Samples were harvested for de termination of liver damage, inflammation and changes in carbohydrate and lipid metabolism.

Results. In LFD-fed control mice, chloroethanol did not cause any significant changes to the liver. In HFD-fed mice, chloroethanol induced significant liver damage and inflammation. Moreover, steatosis, hepatocyte ballooning, infiltrating inflammatory cells and hepatic expression of proinflammatory cytokines were observed in this group. Additionally, chloroethanol altered the expression of key genes and proteins involved in carbohydrate and lipid metabolism in animals on a HFD.

Conclusions. Chloroethanol (as a surrogate VC exposure) not only exacerbated liver injury in a '2-hit' paradigm but also caused direct metabolic changes. This serves as proof-of-concept that VC hepatotoxicity may be modified by diet-induced obesity and NAFLD. These data implicate exposure to VC in the development of liver disease in susceptible populations.

BACKGROUND

Over 33% of US adults are obese (BMI ≥ 30) with another 34.2% being overweight (BMI ≥ 25).[1] One of the major health effects of obesity is non-alcoholic fatty liver disease (NAFLD). Indeed, the burden of liver disease has increased in the US in parallel with the obesity epidemic.[2] However, it is assumed that there are other contributing factors (e.g., environmental factors) that determine overall risk for developing the disease.

Vinyl chloride is found in significant concentrations in the ambient air and the ground water surrounding manufacturing complexes. Therefore, exposure to VC is widespread in industrialized nations. Historically VC-exposure has been associated with hemangiosarcoma, HCC and fibrosis. The Louisville industrial area ('Rubbertown') is a well documented site for VC-induced liver diseases.[3] What is unknown is what low level (sub-NOAEL) exposure will do to the risk of underlying liver diseases. While it is clear that high doses of VC are directly hepatotoxic to humans, the effects of lower doses of VC and its interactions with over nutrition on overall liver health have not been determined.

The risk for developing fatty liver disease is not based solely on one factor, but rather is modified by other mitigating conditions, such as genetic (e.g., polymorphisms in key genes) or environmental (e.g., diet, lifestyle, etc) factors. Numerous studies have now established that physiological/biochemical changes to liver that are pathologically inert can become hepatotoxic in response to a second agent. This '2-hit' paradigm has been best exemplified in non-alcoholic fatty liver diseases.[4] We propose that low-dose VC may also serve as a second hit. The metabolism of VC is similar to that of ethanol, which also causes fatty liver disease. VC is metabolized via an CYP2E1 and aldehyde dehydrogenase dependent pathway. Indeed, a key pathologic characteristic of VC-induced TASH in humans is steatohepatitis analogous to ASH or NASH. VC-metabolites may therefore be important mediators of VC-enhanced NAFLD.

MATERIALS AND METHODS

Animals and treatments. Six week old male C57BL/6J mice were obtained from Jackson Laboratory (Bar Harbor, ME). Animals were fed either a low fat diet (LFD, 13% milk fat) or a high fat diet (HFD, 42% milk fat) for 10 weeks. At the end of this period, animals were administered chloroethanol (50 mg/kg i.g.). They were anesthetized with ketamine/xylazine (100/15 mg/kg, i.m.) 24h after chloroethanol gavage. Animals were sacrificed and blood and tissue were collected for further analyses.

Biochemical analyses and histology. Plasma levels of ALT, AST were determined using standard kits (Thermotrace, Melbourne, Australia). Lipids were extracted from liver tissue samples and resuspended in 200µL 5% lipid free BSA. Triglyceride and cholesterol levels were determined from the samples. Paraffin-embedded sections of liver were stained with hematoxylin & eosin (H&E) to assess overall hepatic structure, and Periodic acid-Schiff reagent (PAS) to detect glycogen.

RNA isolation and real-time RT-PCR. Total RNA was extracted from liver tissue samples by a guanidium thiocyanate-base method (RNA STAT 60 Tel-Test). 1 µg total RNA per sample was reverse transcribed. PCR was performed using the ABI StepOne Plus. The comparative C_T method was used to determine fold differences between samples.

Statistics. Summary data represent means ± SEM (n = 4-6). ANOVA with Bonferroni's post-hoc test or the Mann-Whitney rank sum test was used for the determination of statistical significance among treatment groups, as appropriate. [a], $p < 0.05$ compared to vehicle; [b], $p < 0.05$ compared to animals exposed LPS alone.

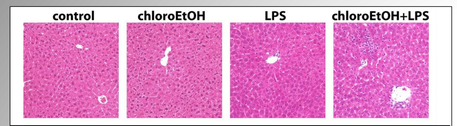

	chloroEtOH vs Control	chloroEtOH + LPS vs LPS
Liver damage	↔	↑
Inflammation	↔	↑
Cell death	↔	↑
- Apoptosis	↔	↓
- Necrosis	↔	↑
Oxidative Stress	↑	↑
Lipids	↑	↑
Glycogen	↓	↓
AMPK	↑	↔
mTOR	↑	↔

Figure 1: ChloroEtOH sensitizes the liver to injury and inflammation. In a previous study, we showed that chloroEtOH by itself caused no gross morphologic changes, but enhanced LPS-induced liver injury and inflammation. This was likely due, in part, to a 'pseudo-fasted state' caused by chloroEtOH; this state was characterized by an increase in lipid storage and decrease of glycogen by concomitant activation of the normally opposed kinases, AMPK and mTOR, which are master metabolic regulators.

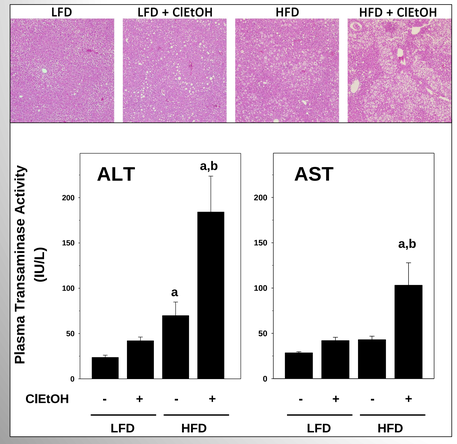

Figure 2: Effect of HFD and chloroEtOH on plasma transaminases. Mice were treated as described in *Materials and Methods*. Alanine aminotransferase (ALT) and aspartate aminotransferase (AST) were determined in plasma samples collected 24 hours after chloroEtOH.

Whereas having no effect in absence of HFD, ClEtOH strongly increased plasma levels of indices of liver damage (AST, ALT) 24 hours after chloroEtOH.

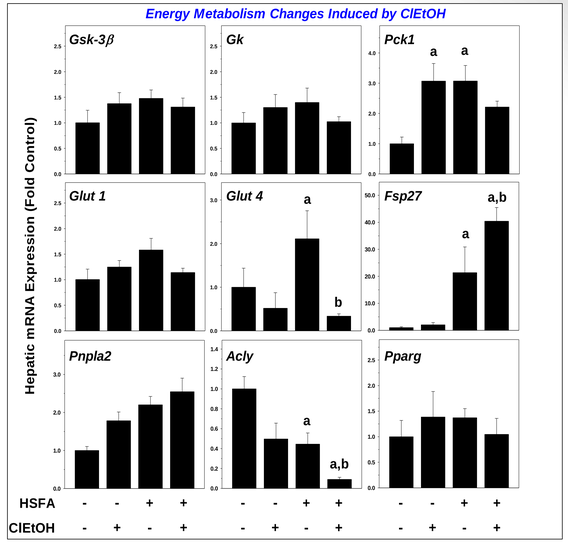

Figure 3: Effect of HFD and ClEtOH on energy metabolism regulating genes. Mice were treated as described in *Materials and Methods* and real-Time RT-PCR for genes regulating carbohydrate and lipid metabolism was performed as described in *Materials and Methods*.

While ClEtOH didn't affect glycogen synthase kinase 3 (Gsk3), glucokinase, phosphoenolpyruvate carboxykinase (Pck1), and Glucose transporter 1 (Glut1), it significantly blunted the expression of glucose transporter 4 (Glut4) when compared to the HFD group. ATP citrate lyase (Acyl) expression was decreased by chloroEtOH alone and in animals fed HSFA, this effect was further enhanced by chloroEtOH. HFD significantly increased the expression of fat-specific protein 27 (Fsp27) and ClEtOH significantly enhanced this effect.

No significant changes in expression was noted in peroxisome proliferator-activated receptor gamma (Pparg; transcriptionally regulates Fsp27 expression) or patatin-like phospholipase domain containing 2 (Pnpla2), a gene shown to be involved in NAFLD.

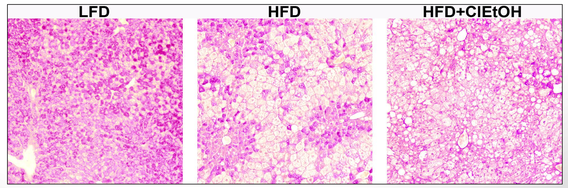

Figure 4: Effect of HFD and chloroEtOH on hepatic glycogen. Mice were treated as described in *Materials and Methods*. Representative photo-micrographs of Periodic acid-Schiff stain (PAS) for glycogen are shown.

Whereas HFD dramatically increases fat accumulation in the liver it has no apparent effect on hepatic glycogen levels. ChloroEtOH depleted unfasted glycogen reserves in the livers of animals fed a HFD.

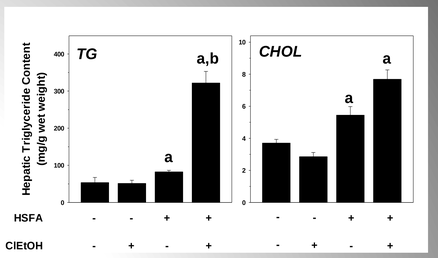

Figure 5: ClEtOH increases hepatic lipid levels. Mice were treated as described in *Materials and Methods* and triglyceride and cholesterol concentrations were determined from extracted lipid samples as described in *Materials and Methods*.

ChloroEtOH alone didn't affect triglyceride or cholesterol concentrations. Animals fed HSFA had significantly higher concentrations of triglyceride and cholesterol and this effect was significantly enhanced with chloroEtOH.

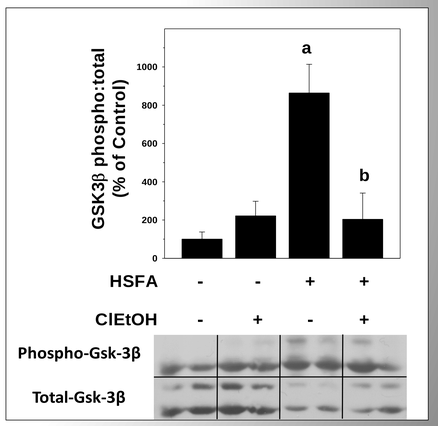

Figure 6: Western blot analysis. Mice were treated as described in *Materials and Methods* and Western Blot analysis was performed as described in *Materials and Methods.*

HFD significantly increased the concentration of Gsk-3β, but ClEtOH blunted the effect of HFD in Western blot analysis.

FUNDING SUPPORT

This research was supported in part by NCI (R25-CA134283 - HY), NIDDK (JIB; CJM), NIEHS (MC), NIAAA (CJM), and the Veterans Administration (MC, CJM).

SUMMARY

Vinyl chloride metabolite chloroEtOH sensitizes the liver to:

1) inflammation
2) Steatosis
3) glycogen depletion
4) Metabolic changes

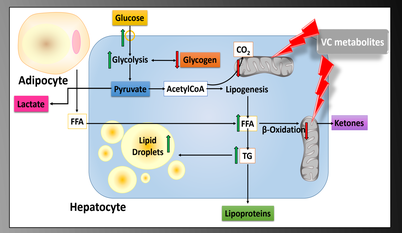

Figure 7: Working Hypothesis. VC metabolites cause mitochondrial damage, which impairs oxidative phosphorylation; the cell increases flux through anaerobic glycolysis to compensate for this loss of ATP yield. The increased demand for glucose depletes glycogen stores and the cell becomes 'pseudo-fasted;' this latter state likely increases AMPK activity. Interestingly, mTOR, which is usually regulated in opposition to AMPK, also appears to be activated by VC exposure. This concomitant activation of catabolic (AMPK) and anabolic (mTOR) signals likely explains why acetylCoA is being shunted to lipid synthesis instead of β-oxidation, even under conditions of ATP depletion. VC also enhanced ER stress after fat accumulation in the cells that was not directly caused by the compound per se. These data therefore may explain why fatty livers are more sensitive to VC/metabolite exposure. The combined metabolic stress of VC exposure likely sensitizes the hepatocyte to oncotic cell death caused by inflammation.

REFERENCES

1. Cave,M., Deaciuc,I., Mendez,C., Song,Z., Joshi-Barve,S., Barve,S. & McClain,C. Nonalcoholic fatty liver disease: predisposing factors and the role of nutrition. *J. Nutr. Biochem.* 18, 184-195 (2007).
2. Cave M et al., Toxicant associated steatohepatitis in vinyl chloride workers. Hepatology. 51:474-81 (2010).
3. Day,C.P. & James,O.F. Steatohepatitis: a tale of two "hits"? *Gastroenterology.* 114, 842-845 (1998).
4. Flegal,K.M., Carroll,M.D., Ogden,C.L. & Curtin,L.R. Prevalence and trends in obesity among US adults, 1999-2008. *JAMA.* 303, 235-241 (2010).